Seismic Enhancement of Welded Unreinforced Flange-Bolted Web Steel Moment Connections

Machel Leigh Morrison¹; Douglas Quinn Schweizer²; and Tasnim Hassan³

Abstract: Widespread damage to welded unreinforced flange-bolted web (WUF-B) steel moment connections during the 1994 Northridge earthquake led to intensive research study of this connection. Despite the improvements to weld metal and connection details, the post-Northridge WUF-B connection was unable to attain sufficient ductility for use in special moment frames (SMFs). This study presents detailed finite element (FE) analysis of post-Northridge WUF-B connections to better understand the mechanisms which limited connection ductility in laboratory tests. Observations made from the FE analysis led to the development and numerical study of a modified WUF-B connection that combines a new bolted web design with a recently validated technique to promote plastic hinging of the beam away from the connection joint. The proposed connection provides the benefit of reduced field welding and UT inspection without sacrificing connection ductility and seismic performance. Finally, the proposed connection is experimentally validated through full-scale seismic testing. The pilot test specimen exceeded the AISC 341 qualifying 4% interstory drift angle without significant strength loss. No weld or near-weld cracks were observed. Instead, failure of the connection resulted from large local buckling deformation in the plastic hinge away from the welded joint. **DOI: 10.1061/(ASCE)ST.1943-541X.0001575.** © 2016 American Society of Civil Engineers.

Author keywords: Steel moment connection; Seismic performance enhancement; Beam plastic hinge; Heat-treated beam section; Reduced beam section; Modified WUF-B; Metal and composite structures.

Introduction

Prior to the 1994 Northridge Earthquake, welded unreinforced flange-bolted web connections (WUF-B) were one of the most commonly used moment connections in earthquake-prone regions of the United States (Bruneau et al. 1998). Investigations after the Northridge Earthquake uncovered widespread damage to WUF-B connections in the form of weld or near weld fractures with little evidence of inelastic action (Bruneau et al. 1998). The widespread use of the WUF-B for several years prior to Northridge has been attributed to its perceived performance (ductility) and economy (Bruneau et al. 1998); in addition, the WUF-B, which was commonly referred to as the "prescriptive connection," was prequalified for seismic applications in the 1988 Uniform Building Code (ICBO 1988) and later adopted into the 1992 AISC Seismic Provisions (AISC 1992). This prequalification was based upon nonstandardized laboratory testing carried out during the 1970s and 1980s (Popov and Stephen 1972; Popov et al. 1985). However, an objective review of results from these and other laboratory tests of WUF-B connections preceding the Northridge earthquake reveals that the performance of WUF-B connections showed considerable inconsistency (Engelhardt and Husain 1993) and perhaps was given perfunctory treatment by building code officials and structural engineers.

Early testing done by Popov and Stephen (1972), in which direct comparisons were made between WUF-B connections and all-welded connections (welded flange-welded web) showed this variability. Of the six WUF-B specimens all but one failed by weld or near-weld fractures. Subsequent studies by Popov et al. (1985) and Engelhardt and Hussain (1993) showed similar failure modes and in many cases abrupt failures with little inelastic action. Several experimental studies conducted after the Northridge earthquake (Sabol et al. 1996; Popov et al. 1998; SAC 2000d) showed similar weld or near-weld fractures of the pre-Northridge WUF-B at very low drift angles.

Post-Northridge studies by Stojadinović et al. (2000) showed that the use of notch tough electrodes combined with improved details such as the removal of the bottom flange backing bar improved connection ductility. However, despite these improvements, the so-called SAC-post-Northridge connection [Fig. 1(a)] did not exceed the AISC *Seismic Provisions* (AISC 1997) 0.03 rad total plastic rotation performance requirement for use in special moment frames (SMFs). Notwithstanding, the study provided informative and insightful results about the behavior and failure mechanism of WUF-B connections constructed with sound welding details, practice, and consumables. Most notably, the failure mode change from brittle weld metal fractures (observed in pre-Northridge WUF-B connections) to ductile tearing followed by fast fracture of the base metal (at the access hole where the beam web meets the beam flange) as shown in Fig. 1(b).

This failure mechanism was repeated for several specimens and was independent of the beam and column sizes (SAC 2000d). Similar failures were also observed in WUF-B specimens with an improved access hole geometry (Han et al. 2007), designed to lower stress and strain concentrations. Despite this design improvement, fractures at the access hole similar to those shown in Fig. 1(b) were observed, which suggests that this failure mechanism may not be very sensitive to access hole design. These results reinforce the suggestion made by Stojadinović et al. (2000) that moment connections intended for use in SMFs should incorporate

¹Postdoctoral Research Scholar, Dept. of Civil, Construction and Environmental Engineering, North Carolina State Univ., Raleigh, NC 27607 (corresponding author). E-mail: mlmorris@ncsu.edu

²Senior Engineer, Thorton Tomasetti, Washington, DC 20036.

³Professor, Dept. of Civil, Construction and Environmental Engineering, North Carolina State Univ., Raleigh, NC 27607.

Note. This manuscript was submitted on October 30, 2015; approved on March 21, 2016; published online on June 6, 2016. Discussion period open until November 6, 2016; separate discussions must be submitted for individual papers. This paper is part of the *Journal of Structural Engineering*, © ASCE, ISSN 0733-9445.

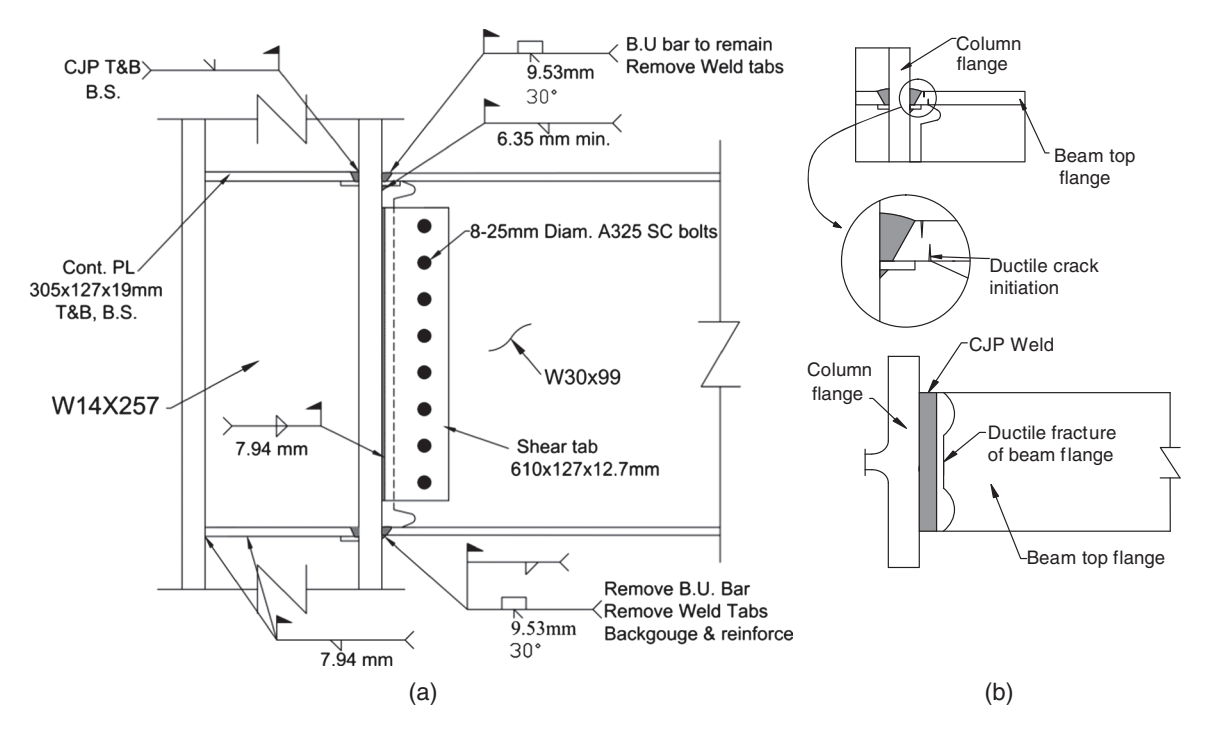


Fig. 1. (a) Post-Northridge WUF-B connection (Specimen 6.1; data from SAC 2000d); (b) sketch of ductile fracture failure of Specimen 6.1

both "weld fracture mitigation measures and flange overstress mitigation measures."

A flange overstress mitigation measure which has found wide-spread use in current practice is the reduced beam section (RBS). In RBS moment connections, the beam is weakened by selective trimming of the flanges adjacent to the column face so as to force plastic hinging to occur away from the welded joint. However, combination of the RBS with a bolted web connection (RBS-B) has yielded mixed results; achieving 4% drift or higher with (in some cases) eventual weld or near-weld failures (Iwankiw and Carter 1996; SAC 2000a) and unable to attain 4% drift (Lee et al. 2005), suffering failures at the access hole in repeated tests. As a result, like the WUF-B, RBS connections with bolted webs have not been prequalified for use in SMFs.

In several studies on WUF-B and RBS-B connections, it has been noted that slip of the web bolts is observed early in the inelastic cycles, causing a reduction of moment strength (Krawinkler and Popov 1982; Lee et al. 2005; Han et al. 2007). More importantly, slippage of the web bolts means that there will be rigid rotation of the beam web (in the connection region) and redistribution of web bending stresses to the flanges. This places larger demands on the beam flanges adjacent to the connection, leading to a higher incidence of near-weld failure (Engelhardt and Sabol 1997). Indeed, higher axial strain demands in the beam flanges adjacent to the connection have been recorded in RBS-B connections when compared to nominally identical RBS connections with welded webs (Lee et al. 2005), which provides evidence of stress redistribution.

Perceptions about the debilitating effect of bolt slippage on the performance of WUF-B and RBS-B connections have been developed mainly through qualitative comparison of bolted web and welded web specimens in experimental studies (Popov and Stephen 1972; SAC 2000a; Lee et al. 2005). However, the effect has not been analyzed in detail experimentally or analytically. In this study, detailed finite element analysis has been conducted to quantify the effect of the bolted web attachment on global and local responses of WUF-B connections. By predicting global and local responses, improved understanding of connection behavior and failure

mechanisms is attained. This facilitated the development and experimental validation (through full-scale testing) of an improved design to enhance seismic performance of WUF-B connections as presented subsequently.

Finite Element Modeling

Three-dimensional nonlinear finite element (FE) models were developed for WUF-B connections using the commercial FE analysis software ANSYS Mechanical ADPL. Geometric, material, and contact nonlinearities were incorporated in the finite element models. An example of the finite element mesh and boundary conditions is shown in Figs. 2(a and b). The beam, column, shear tabs, and continuity plates were modeled with eight-noded solid hexahedral elements (SOLID185) with selective reduced integration, whereas high-strength bolts were modeled with 20-noded solid hexahedral elements (SOLID186) with uniform reduced integration. Bolt holes were assumed to be 1.6 mm (1/16 in.) larger than the bolt diameter. The AISC (2005) specified minimum bolt pretension forces were generated via a "pretension element" (PREST 179), which inserts one-dimensional zero-length elements at the nodes of a specified cross section of the bolt shank. When pretension loading is applied, this element simulates the reduction of effective length (length between the underside of the bolt head and nut), which occurs during tightening of the fastener. In the simulation, the pretension load/ clamping force is applied first and stored as an initial displacement before the application of loads at the beam tip. This allows for the simulation of fluctuations to the initial pretension load due to the deformations and interactions of the assembly. It should be noted, however, that the bolt threads were not modeled in this study, i.e., the bolt nut was glued to the bolt shank. Similar approaches to modeling structural bolts have been used in previous studies (Rahman et al. 2007).

The interactions among the bolts, shear tab, and beam web were modeled by deformable surface-to-surface sliding contact pairs (CONTA174) using the augmented Lagrangian contact algorithm

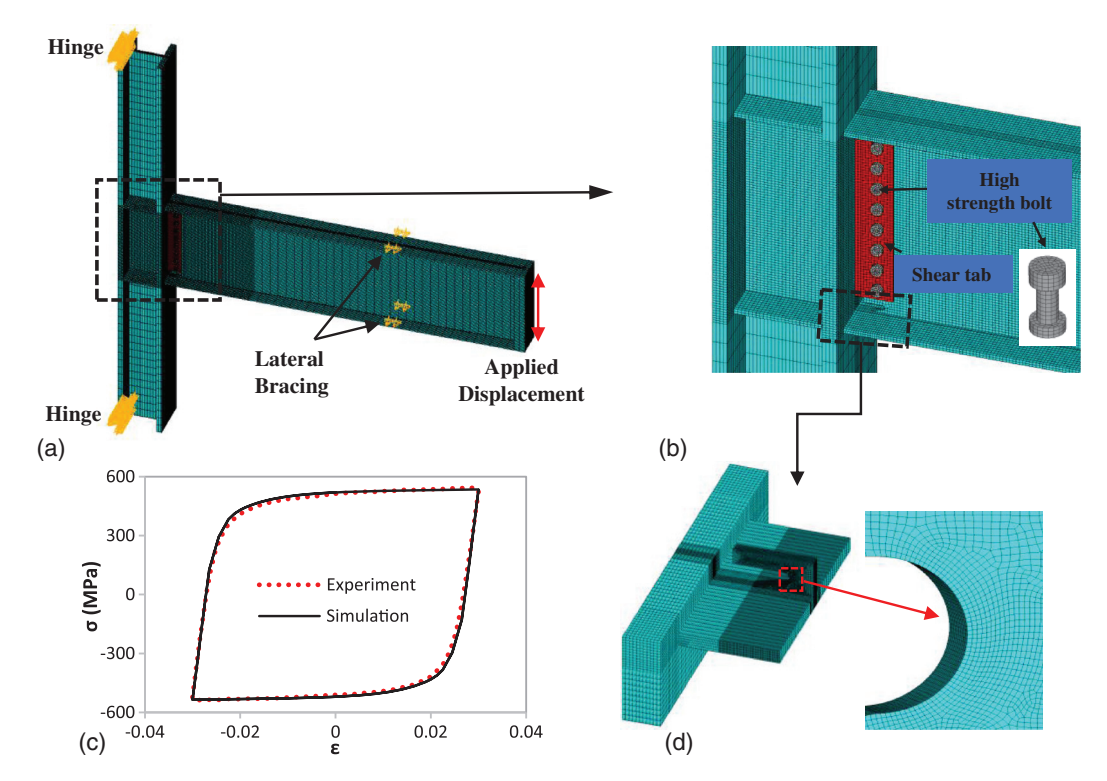


Fig. 2. (a) Specimen 6.1 FE mesh and boundary condtions; (b) close up view of mesh; (c) fitted ASTM A572 gr 50 hystersis curve (data from Kaufmann et al. 2001); (d) FE submodel mesh

with a normal contact stiffness factor of 0.1. Coulomb friction was used to model the sticking/sliding interactions of the faying surfaces. The limiting coefficients of static friction for the assumed faying surface conditions were obtained from the AISC *Steel Construction Manual* (AISC 2005). More details on the treatment of contact modeling including validation of the modeling approach to predict bolt slip are presented in Morrison (2015).

Material and Geometric Nonlinearities

Finite element models accounted for material nonlinearity through rate-independent metal plasticity theory based on the von Mises yield criterion, additive strain decomposition, and the associated flow rule. A multilinear kinematic hardening model calibrated from uniaxial monotonic tensile tests performed by Kaufmann et al. (2001) and Morrison (2015) was used for monotonic simulations, whereas the Chaboche nonlinear kinematic hardening model (Chaboche 1986) was used for cyclic analysis. Chaboche material model parameters were obtained by fitting stable hysteresis loops as shown in Fig. 2(c). A distinguishing feature of the Chaboche model is the superposition of multiple nonlinear kinematic hardening rules. This allows for accurate simulation of hysteretic loop shape and therefore plastic modulus over a wide strain range. A summary of the material model parameters used for cyclic analysis is provided in Table 1.

Geometric nonlinearities were accounted for via a large deformation formulation that, accompanied by small eccentricities/imperfections in the geometry, allowed for the simulation of local

Table 1. FE Constitutive Model and CVGM Parameters

Туре	Constitutive model parameters	A572 Gr. 50	A992	Heat-treated A992	High-strength bolt	E70 weld ^a
Elastic parameters	E (GPa)	200	200	200	200	200
1	σ_0 (MPa)	323	239	172.4	777.7	572
	ν	0.3	0.3	0.3	0.3	0.3
Kinematic hardening parameters	C_1 (MPa)	106,703	383,337	159,018	204,616	1,450
	C_2 (MPa)	11,300	280,782	99,791	152,250	_
	C_3 (MPa)	275.8	50,780	60,553	101,319	_
	C_4 (MPa)	34.5	1,958	1,218	32,219	_
	γ_1	893	21,081	26,410	4,143	55
	γ_2	134	6,256	3,674	285	_
	γ_3	4	515	622	107	_
	γ_A	0	13	0	0	_
CVGM ^b	VGI _{monotonic}	2.8^{b}	_	_	_	_
Parameters	λ	0.38^{b}	_	_	_	_

^aParameters obtained from Myers (2009).

^bParameters obtained from Kanvinde and Deierlein (2007).

buckling. WUF-B connections contain eccentricity due to the offset of the shear tab from the centerline of the column, so no additional imperfections were necessary to perturb local buckling. However, in the case of all-welded connections (welded flange-welded web), initial geometric imperfections were introduced to perturb local buckling. It is noted that due to the symmetry of the mesh, boundary conditions, loads, and resulting deformations, local buckling could not be simulated and unrealistically high values of peak strength were predicted when initial geometric imperfections were not considered. Initial imperfections were obtained by first conducting an eigenvalue analysis of the perfect structure and then prescribing a scaled value of the first eigenmode displacement field as the initial configuration of the structure. The maximum value of geometric imperfection was 1.3 mm (0.05 in.), which was chosen to represent reasonable values of W-shape "out of squareness" based on ASTM A6 (ASTM 2010) tolerances. Similar approaches have been used in SAC (1998).

Finite Element Submodel and Cyclic Void Growth Damage Model

Submodels of both the top and bottom beam flange to column flange connections were developed to study with better accuracy and resolution local stress and strain responses in the weld toe and access hole region. An example of the submodel mesh used for the beam bottom flange to column flange connection is shown in Fig. 2(d). Mesh sensitivity studies showed that the chosen element edge size of approximately 0.2 mm in the regions of interest in the FE submodels was sufficient to accurately capture stresses and strains. Stress and strain indices from this submodel were used as inputs to a cyclic void growth model (CVGM) proposed by Kanvinde and Deierlein (2007) to predict the initiation of ductile macroscopic cracks that were reported during laboratory tests (Stojadinović et al. 2000; SAC 2000d, b).

To date several journal articles discussing the CVGM details, development, and applications have been published (Kanvinde and Deierlein 2007, 2008). As such, details of the model are not repeated here. However, it should be emphasized that the CVGM was developed to predicted ultra-low cycle fatigue (ULCF) failure in high-stress triaxiality conditions. ULCF failure occurs at larger inelastic strains and lower cycle counts as compared to low cycle fatigue failures and displays common characteristics with ductile fracture from monotonic loading (Kanvinde and Deierlein 2007). It is used in this study because failures observed in lab testing of WUF-B connections seem to fall in the category of ULCF based on the low number of cycles to fracture, the reported appearance of the fracture surface (SAC 2000d, b), the large inelastic strains recorded (SAC 2000d), and the relatively high stress triaxiality ratios calculated near the fracture location.

Manufacturing and welding-induced residual stresses or stress concentrations created by pre-existing voids or cracks were not considered in the submodel. Heterogeneity of the material properties in the heat-affected zone (HAZ) was also excluded. As a result of these idealizations, it was found that gradients of stress and strain around the assumed flaw-free semicircular access hole and weld toe regions were not sharp relative to the 0.2 mm "characteristic length" or length scale (Kanvinde and Deierlein 2008) representative of the physical events leading to ductile fracture in A572 gr. 50 steel. Therefore, once the fracture condition was satisfied at an element integration point, it was simultaneously satisfied over a volume larger than that defined by the characteristic length. As a result, ductile fracture prediction was insensitive to the 0.2 mm characteristic length and pointwise satisfaction of the fracture criteria was sufficient.

Finally, it should be stated that the numerical model does not address crack propagation; instead, the CVGM is used to predict the initiation of a macroscopic crack based on existing stress and strain conditions. The CVGM is thus "uncoupled" from the FE analysis and does not affect the global or local response predictions. As a result, loss of connection strength due to ductile tearing and fast fracture was not captured.

FE Model Validation

For FE model validation, Specimen 6.1 [Fig. 1(a)] tested by Stojadinović et al. (2000) was modeled. Displacements were applied 3.4 m (134 in.) from the column face at the beam tip according to the loading protocol reported in SAC (2000d). The predicted moment-rotation response (calculated at the column centerline) is plotted against the experimental response in Fig. 3(a). The model prediction is found to be in close agreement with the experimental response, which is partly attributed to the detailed modeling of the bolted shear tab web connection. To demonstrate the importance of this modeling detail, the simulated moment-rotation response for a connection with the beam web assumed to be monolithic (glued) with the shear tab is plotted against the experimental response in Fig. 3(b). This resulted in overprediction of moment responses and an overall "stiffer" prediction, which has been observed in previous studies where this modeling simplification was made (SAC 1998; Popov et al. 1998).

The evolution of the void growth indices (for the CVGM) which were calculated from stress and strain data extracted from the submodel of Specimen 6.1 are shown in Fig. 3(c). The location considered is the center of the web-to-flange intersection at the weld access hole on the inside surface of the beam top flange shown in Fig. 3(d). This and other locations such as the center and edges of the beam flange at the weld toe were evaluated for satisfaction of the CVGM fracture criteria. However, failure was predicted (i.e., $VGI_{cyclic} > VGI_{cyclic}^{critical}$) earliest in this location which corresponds to the location of highest plastic strain and is in agreement with the reported fracture initiation location in the experiment (SAC 2000d, b). Note that fracture initiation is predicted to occur at the end of the second excursion of loading at 2% drift, whereas fracture was observed slightly before the end of the second excursion at 2% drift.

Monotonic Analysis and Comparative Study of Post-Northridge WUF-B Connections

The monotonic moment versus rotation response of the WUF-B connection [shown in Fig. 1(a)] was simulated and compared to that of an all-welded connection (welded flange-welded web) of identical geometry to demonstrate the effect of web bolt slippage on post-Northridge WUF-B connections. The simulated responses are compared in Fig. 4(a). In the figure, moments and rotations are calculated at the column face (the assumed plastic hinge location) to evaluate the capability of connections to develop the flexural strength of the beam.

From Fig. 4(a) it is observed that initially both connections display similar linear behavior with comparable elastic stiffness. However, the onset of nonlinear behavior occurs earlier and more abruptly for the WUF-B connection. This sudden change in stiffness occurs at a smaller bending moment than the calculated yield moment (M_y) as a result of bolt slippage and subsequent yielding of the beam flanges. The WUF-B connection displays very low post-yield stiffness until approximately 0.02 radians rotation when the outer two bolts begin to bear against the holes of the shear tab and

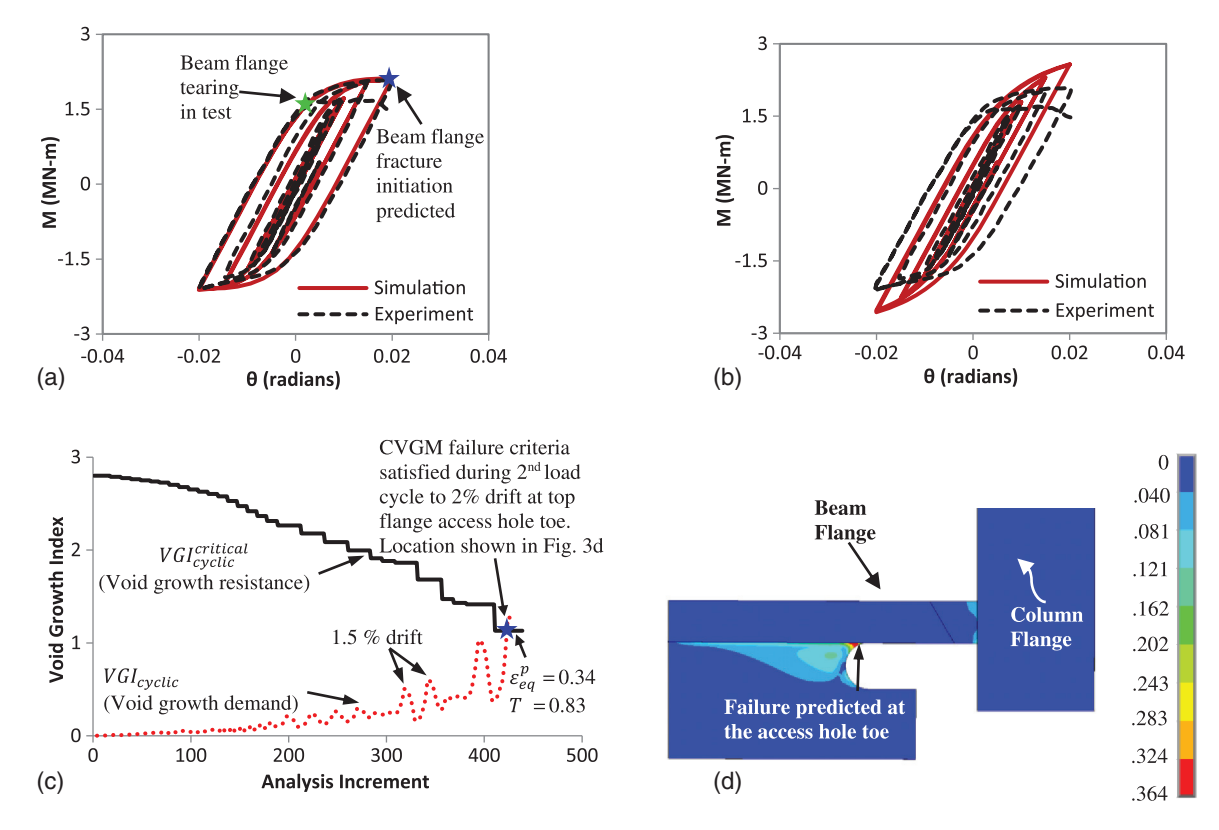


Fig. 3. FE analysis of Specimen 6.1: (a) comparison of experiment and detailed simulation; (b) comparison of experiment and simplified simulation; (c) CVGM failure prediction at the toe of the access hole [shown in Fig. 3(d)]; (d) equivalent plastic strain contour from submodel; note ε_{eq}^p = equivalent plastic strain; T = stress triaxiality

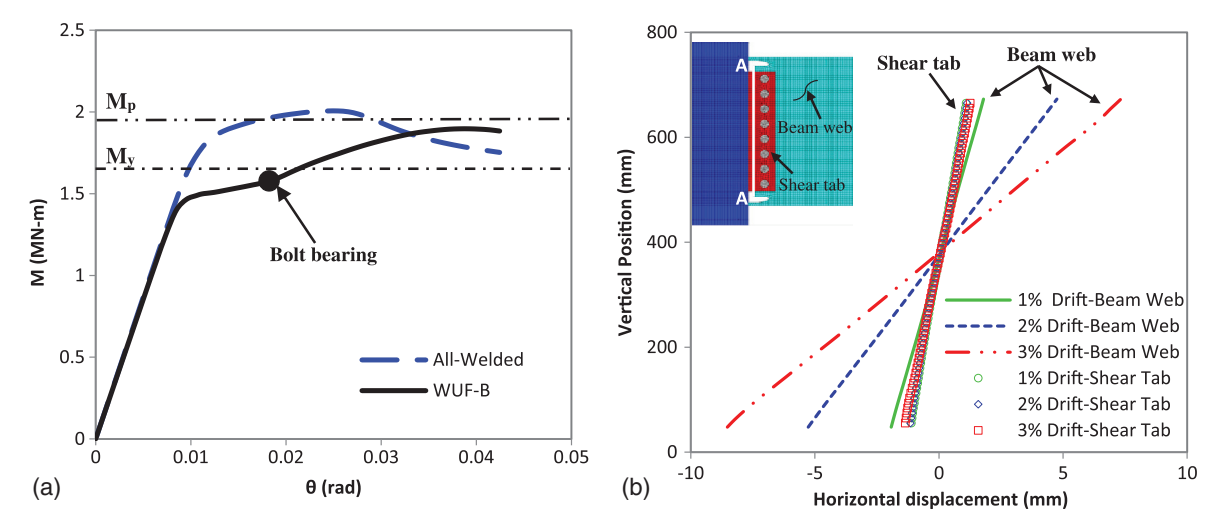


Fig. 4. Comparison of FE monotonic response prediction for WUF-B and all-welded moment connections: (a) moment-rotation responses; (b) horizontal displacements of the beam web and shear tab along line A-A

beam web. At this point there is a discernible increase in stiffness and the connection resistance continues to increase up to 0.04 radians. As shown in Fig. 4(a) the WUF-B connection does not attain the calculated plastic moment capacity (M_p) of the beam section at the column face.

On the other hand, the all-welded connection displays the "characteristic" response of fully restrained steel moment connections. The onset of nonlinear moment-rotation behavior begins at the calculated yield moment, and the connection displays gradual reduction of stiffness thereafter. In contrast to the WUF-B connection,

the all-welded connection exceeds the calculated plastic moment capacity at the column face. The onset of strength degradation occurs earlier in the all-welded connection due to the larger flexural stresses developed in the beam web adjacent to the connection. As a result, web local buckling is initiated that triggers flange local buckling and twisting of the cross section leading to strength degradation.

From the previously described moment-rotation response it is clear that bolt slippage has a debilitating effect on the global behavior of the WUF-B connection. Bolt slippage also has detrimental

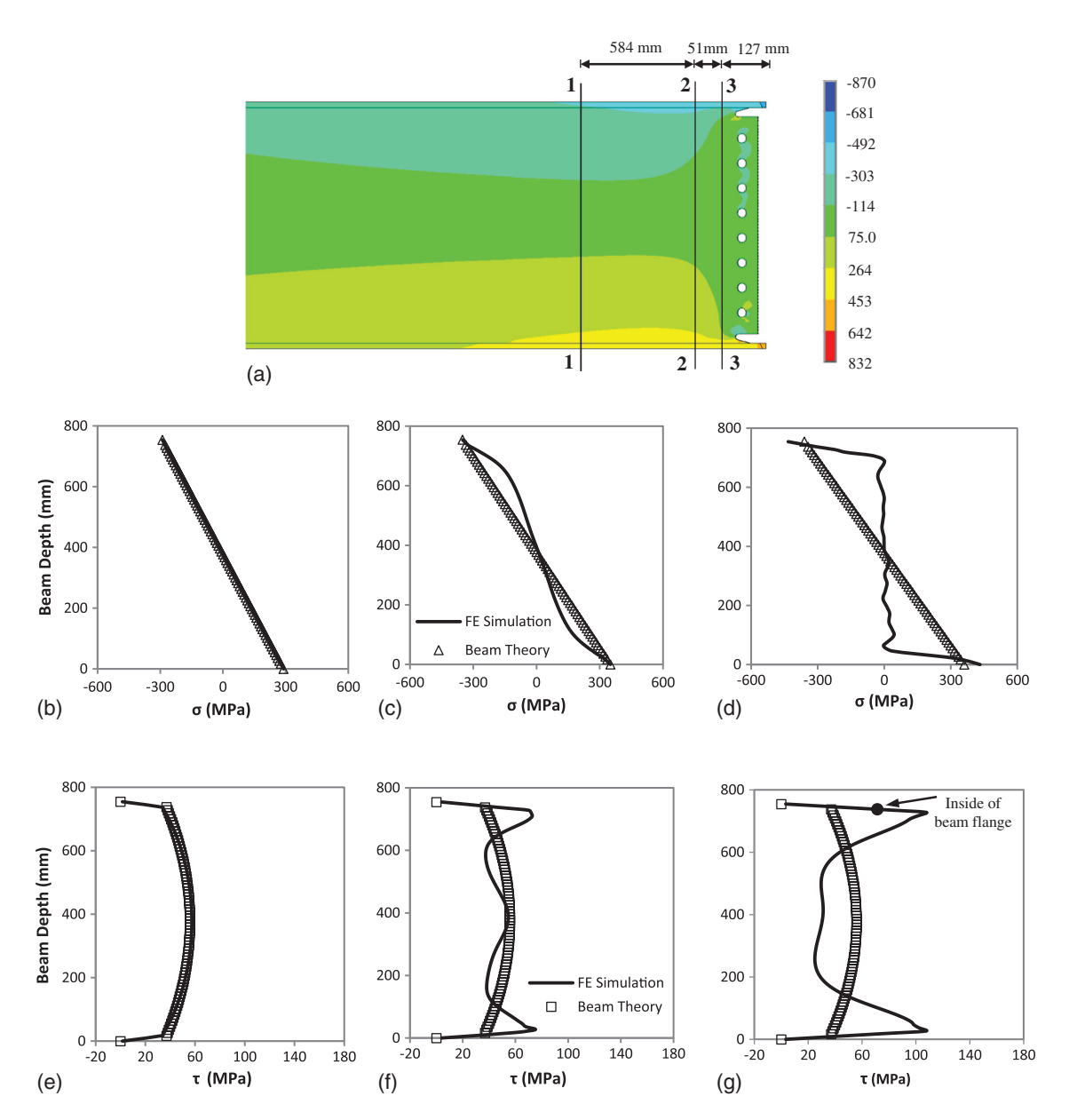


Fig. 5. FE Simulation and beam theory stresses in WUF-B at applied moment M_y : (a) contour plot of flexural stress; flexural stresses at section (b) 1-1; (c) 2-2; (d) 3-3; vertical shear stresses at section (e) 1-1; (f) 2-2; (g) 3-3

effects on the local stresses and strains in the connection region. To illustrate web bolt slippage progression, Fig. 4(b) compares the horizontal nodal displacements on the vertical edge of the beam web adjacent to the column flange with the horizontal displacements of adjacent nodes on the shear tab. Note the increasing displacements of the beam web, which vary linearly with depth, compared with the very small displacements of the shear tab. This illustrates the slippage of the beam web with progression of loading. Note that even after the bolts begin to bear against the holes of the shear tab and beam web [at approximately 0.02 radians rotation, see Fig. 4(a)] additional increase in relative displacements between the web and shear tab takes place due to the deformation of the outer two bolt holes.

It is important to keep in mind that the bolted shear tab connection of the post-Northridge WUF-B was designed as a slip-critical connection to resist beam shear only (SAC 2000d). Therefore the poor slip resistance described previously is expected because the geometric arrangement (vertical array) of the bolts

is not efficient in resisting in-plane rotation due to bending moments.

Flexural Stress Distribution in WUF-B and All-Welded Connections

Figs. 5(a) and 6(a) show the contour plot of flexural stress in the WUF-B and all-welded connections respectively at an applied moment equal to the yield moment (M_y). The nodal averaged flexural stresses acting on the centerline of the beam cross section—762 mm (30 in.), 178 mm (7 in.), and 127 mm (5 in.) from the face of the column (sections 1-1, 2-2, and 3-3)—are plotted against those predicted by classical beam theory in Figs. 5(b–d) and 6(b–d). Figs. 5(a–d) show that as a result of bolt slippage, bending stresses in the WUF-B gradually redistribute from the beam web into the flanges near the connection. Note from the contour plot [Fig. 5(a)] that this stress redistribution takes place adjacent to the weld access hole, causing most of the web flexural

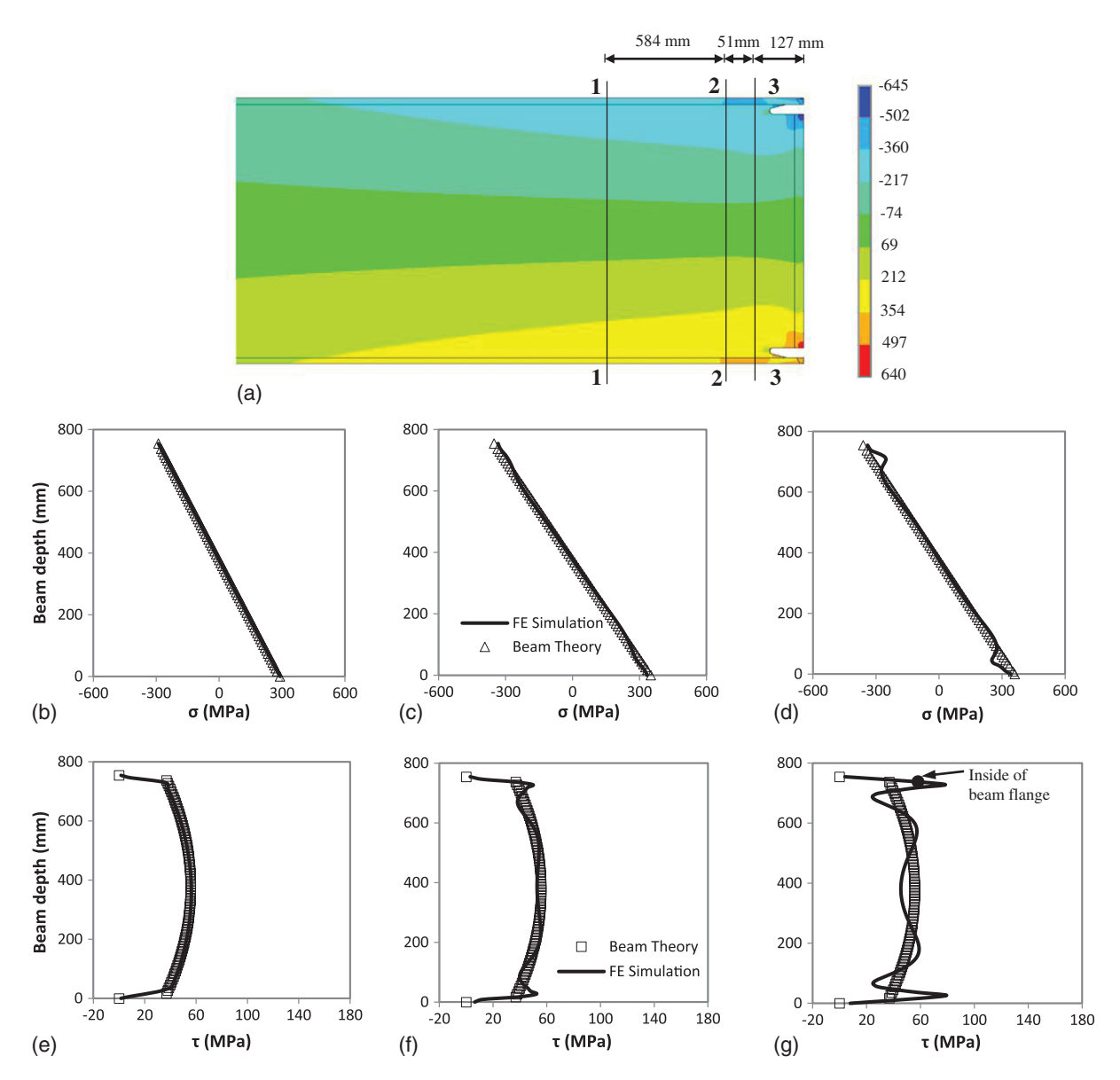


Fig. 6. FE Simulation and beam theory stresses in all-welded at applied moment M_y : (a) contour plot of flexural stress; flexural stresses at section (b) 1-1; (c) 2-2; (d) 3-3; vertical shear stresses at section (e) 1-1; (f) 2-2; (g) 3-3

Table 2. Percent of Shear and Bending Moment Resisted by Beam Flanges at the Column Face

		Connection type									
	WUF-B $(\mu = 0.35)$		$\begin{array}{c} \text{HBS-B} \\ \text{All-welded} & (\mu=0.5) \end{array}$			HBS-W		WUF-B w/HBS $(\mu = 0.35)$			
Drift %	V_f/V (%)	M_f/M (%)	V_f/V (%)	M_f/M (%)	V_f/V (%)	M_f/M (%)	V_f/V (%)	$M_f/M \ (\%)$	V_f/V (%)	M_f/M (%)	
0.5	28	91	24	81	25	84	24	81	29	91	
1	11	89	11	75	24	75	24	71	29	87	
2	11	87	11	69	20	73	24	69	21	87	

Note: M = beam bending moment at column face; $M_f =$ beam bending moment resisted by beam flanges at column face; V = beam shear force; $V_f =$ beam shear force resisted by beam flanges at column face; $\mu =$ limiting coefficient of static friction used between shear tab and beam web in FE model.

stresses to flow around the access hole web copes into the flanges, placing large demands in this region [Fig. 5(d)]. In contrast to the WUF-B, close agreement is obtained between the flexural stress distributions of the all-welded connection and those predicted by classical beam theory at all locations [Figs. 6(b-d)]. The slight disturbance to the stress distribution near to the top and bottom flanges in Figs. 6(c and d) is created by the access hole. The relatively low

stiffness (bending) of the bolted web connection accompanied by bolt slippage led to the flanges of the WUF-B resisting 18% more of the bending moment developed at the column face than the all-welded connection at 2% drift. This is reported in Table 2 where the percentage of shear and bending moment resisted by beam flanges at the column face for various connection designs (discussed more later) are tabulated.

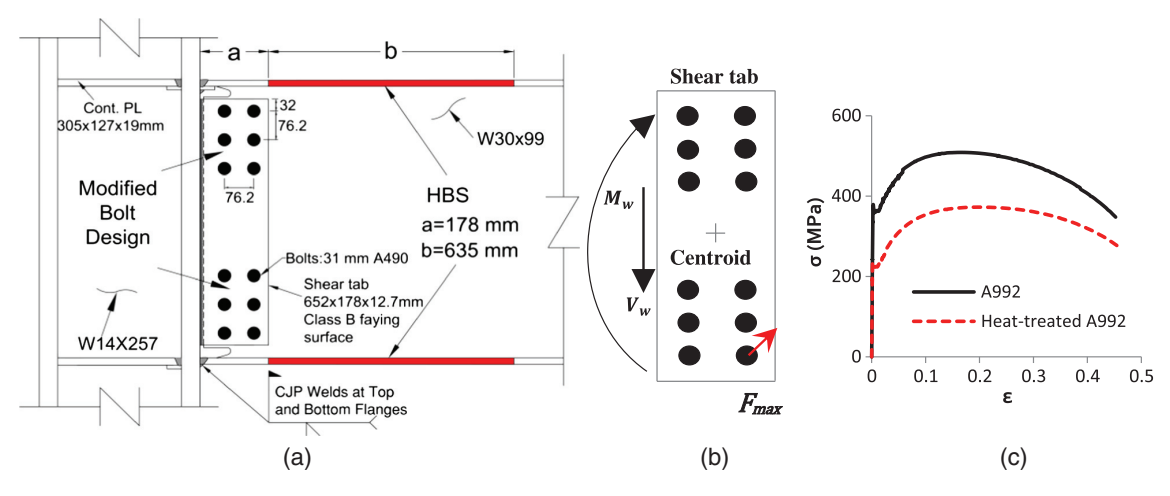


Fig. 7. (a) HBS-B connection (dimensions in mm); (b) free body diagram of shear tab; (c) engineering stress-strain response of A992 and heat-treated A992 steel

Shear Stress Distribution in WUF-B and All-Welded Connections

The nodal averaged vertical shear stresses acting on the centerline of the beam at sections 1-1, 2-2, and 3-3 are compared to classical theory predictions in Figs. 5(e–g) and 6(e–g). Redistribution of the vertical shear stresses take place near the WUF-B and all-welded connections resulting in higher shear stresses at the top and bottom of the beam web and the inside of the beam flange [Figs. 5(f and g) and 6(f and g)]. The redistribution of shear stresses in the connection region is primarily due to boundary restraints to column deformation, Poisson deformation, and shear warping deformation. These boundary effects have been discussed in other studies (Goel et al. 1997; SAC 1998).

Vertical shear stress redistribution results in pronounced local bending of the beam flanges across their width and along their length, which places additional flexural stresses at the access hole toe and at the root of the bottom flange complete joint penetration (CJP) weld. Note that at beam sections 2-2 and 3-3 the redistribution of shear stress in the WUF-B is more pronounced than in the all-welded connection resulting in higher shear stresses [Figs. 5(f and g) and 6(f and g)]. However, at the column face, the beam flanges of the WUF-B don't transmit significantly more shear force than the all-welded connection (Table 2). The higher concentrations of shear stress in the WUF-B are due to the flow of flexural stresses from the beam web to flanges [Figs. 5(a, c, and d)] which cause steep inclination of the principal stress vectors at the top and bottom of the beam web and the inside of the beam flange at cross sections just afore the weld access hole. However, at the column face much of this vertical shear is resisted by the bolted shear tab.

In general, the vertical shear forces carried by the beam flanges at column face are affected by the relative transverse stiffness of the flanges; therefore, thicker flanges will resist a higher portion of beam shear force assuming all else equal. Also, due to tensile stiffening from membrane forces, the tension flange will in general resist higher shear forces than the compression flange. The former of these observations has led to the development of connections such as the slotted web (Richard et al. 1997) and free flange (SAC 2000c), which essentially separate the beam flange from the web for a sufficient distance away from the connection region. Consequently, the transverse flange stiffness is reduced, which in turn lowers the vertical shear force carried by the beam flanges at the column face. It must be noted that despite the presence and adverse effects of shear stress redistribution and consequent shear

forces resisted by beam flanges in the WUF-B and all-welded connections, this effect is blunted when the flanges undergo wide-spread yielding adjacent to the column face, which reduces flange stiffness. As shown in Table 2, the portion of beam shear resisted by the flanges of the WUF-B and all-welded connections reduces by more than 50% as loading progresses from 0.5 to 2% drift. Similar observations have been made by others (SAC 1998).

Seismic Enhancement of WUF-B Moment Connections

The aforementioned results show that due to bolt slippage the flanges of the WUF-B are subjected to substantially higher bending moments, flexural stresses, and shear stresses near the access hole than the all-welded connection. Upon yielding, these stress concentrations become strain concentrations that grow rapidly with applied loading and lead to ductile rupture observed in lab testing (Stojadinović et al. 2000; Han et al. 2007). This mechanism has been deduced from the results of both cyclic and monotonic analysis of the WUF-B connection.

To improve upon the performance of the WUF-B without sacrificing its attractive features (i.e., less field welding and faster erection), two performance enhancement techniques are proposed. The first is a modified bolt design originally proposed by Lee and Kim (2007) in which the bolts are designed to transfer web bending moments and shear forces through friction. To more efficiently resist the web bending moments, the bolts are rearranged to be located toward the outer edges of the beam web as shown in Figs. 7 (a and b). This creates a stiffer web connection leading to reduced redistribution of flexural stresses to the beam flange.

To further reduce the strain concentrations at the weld access hole and weld HAZ, a recently validated technique (Morrison et al. 2015) to promote plastic hinging of the beam by selectively reducing the material strength of the beam flanges away from the connection joint is also incorporated. This material strength reduction is achieved through high temperature heat-treatment (annealing) of the beam flanges in the areas highlighted grey in Fig. 7(a), and the resulting strength reduction is shown in Fig. 7(c). As a consequence of this strength reduction, plastic hinging of the beam takes place in the heat-treated beam section (HBS). Therefore, large displacements applied at the beam tip are mostly accommodated by yielding and plastic hinging of the HBS. This reduces inelastic strain demands at the weld access hole and weld HAZ. In a similar

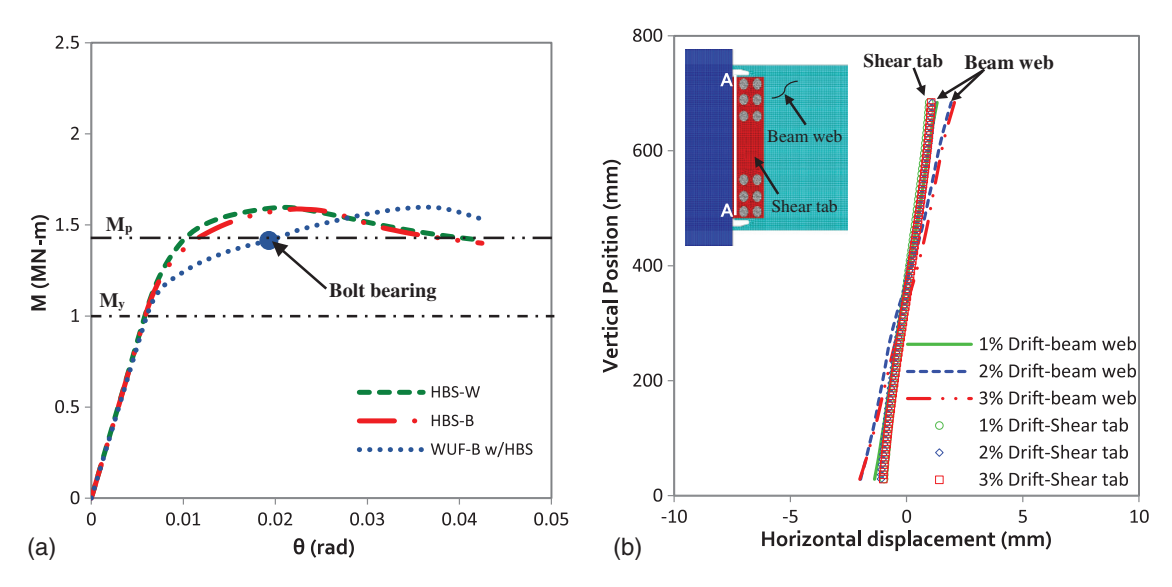


Fig. 8. Comparison of FE monotonic response prediction for HBS-W, HBS-B, and WUF-B w/HBS: (a) moment-rotation responses; (b) horizontal displacements of the beam web and shear tab along line A-A for HBS-B

manner to the RBS, this connection provides a ductile seismic fuse through weakening, but because the elastic modulus of the HBS is unchanged, a connection modified with such a technique does not sacrifice elastic stiffness as does the RBS. Also, because the cross section of the beam is unaltered and the inelastic portion of the stress-strain curve is not significantly modified [note the downward shift of the stress-strain curve in [Fig. 7(c)], the buckling resistance remains similar to that of a beam section before heat treatment.

Finite Element Analysis of Enhanced WUF-B Connections

The monotonic moment versus rotation response of connections with various web connection details, all of which are enhanced with the HBS technique, are plotted and compared in Fig. 8(a). These include an all-welded connection (HBS-W), the proposed modified bolted web connection (HBS-B) shown in Fig. 7(a), and the post-Northridge WUF-B (WUF-B w/HBS). All connections share the same member size, geometry, and boundary conditions as those previously analyzed. Yield moments and plastic moments for connections with HBS were calculated by extrapolating (to the column face) the cross-section yield and plastic moments from the heattreated beam section nearest to the column face [Fig. 7(a)] according to the linear moment gradient. Based on the strength reduction shown in Fig. 7(c) the section yield and plastic moments of the $W30 \times 99$ beam [Fig. 7(a)] were reduced by 38 and 26% respectively from the heat treatment. In the FE analysis the heat-treated regions of the flange are assumed to be homogeneous because the results from tensile coupon tests showed small spatial variation in tensile properties. Detailed design procedures for the bolted shear tab connection of the HBS-B are presented in Morrison (2015).

From Fig. 8(a), benefits obtained from both the HBS and the modified bolt detail are evident. Firstly, by reducing connection moment demands and promoting yielding in the HBS, connection strength appears to be less sensitive to the web connection detail, i.e., all connections exhibit linear behavior to their calculated yield moments and all develop their calculated plastic moment. However, in a comparable manner to the previously studied WUF-B, the WUF-B w/HBS exhibits low postyield stiffness as a result of bolt slippage. The modified bolt design (HBS-B) significantly improves

connection postyield stiffness although it displays slightly lower postyield stiffness than the all-welded connection (HBS-W). This is as a result of very small amounts of bolt slippage (approximately 1 mm by 3% drift) see Fig. 8(b), obtained in this analysis. Although the effect of this slippage is noticeable, as will be demonstrated later, it does not appear to have a considerable effect on the global or local connection behavior and connection resilience. Throughout the load history web moments and shear forces were transferred by friction as bolts did not bear against the holes of the beam web and shear tab.

The modified bolt design provides a stiffer web connection and as a result reduces the redistribution of web bending moments and flexural stresses to the beam flanges. This is verified by comparing the moments resisted by the beam flanges of the HBS-B and WUF-B w/HBS at the column face shown in Table 2. In addition, flexural stresses acting on the beam flange at the access hole location (shown in the figure inset) are reduced as shown in Fig. 9(a).

Flange Shear in HBS and RBS Connections

Previously it was noted that the portion of beam shear force resisted by the beam flanges at the column face in WUF-B and all-welded connections is significantly reduced upon widespread yielding of the flanges at the column face. However, connections modified with HBS or RBS don't undergo widespread yielding at the column face; only limited yielding takes place in areas of high stress concentrations (access hole toe, weld toe, etc.). As a result, the portion of beam shear forces resisted by the flanges at the column face in these connections does not significantly change throughout the loading history, as demonstrated for HBS connections in Table 2.

This evidence may shed light on the mixed results of RBS-B connections in lab testing. In studies conducted with W30 \times 99 and W36 \times 150 beams (Iwankiw and Carter 1996; SAC 2000a), they have readily achieved 4% story drift or greater. However, in the study by Lee et al. (2005) in which W27 \times 123 beams were tested, repeated specimens failed to attain 4% drift, suffering brittle flange fractures at the access hole. The W27 \times 123 section is shallower and has thicker flanges (hence higher relative flange stiffness) than both the W30 \times 99 and W36 \times 150 sections. FE analysis of RBS connections (40% flange reduction) with W36 \times 150 and W27 \times 123 beams showed that the flanges of

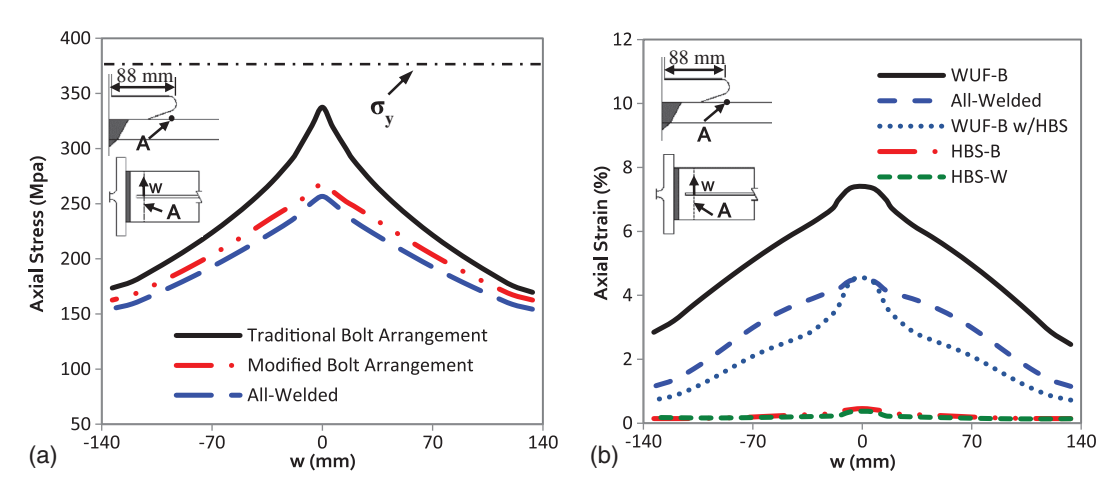


Fig. 9. (a) FE calculated flexural (axial) stress acting on beam flange (240 kN beam tip load applied 3.4 m from the column face to all connections); (b) FE calculated flexural (axial) strains across beam flange at 0.03 rad story drift

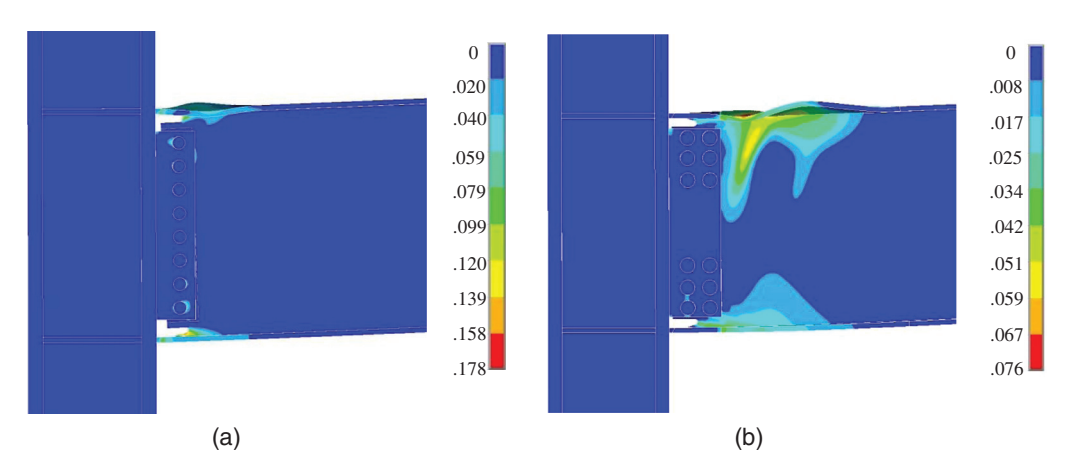


Fig. 10. Equivalent plastic strain contours at 4% drift (monotonic loading) of (a) WUF-B; (b) HBS-B

the W36 \times 150 resist 16% of the beam shear for elastic loading (0.5% drift) which drops to 10% by 2% drift. However, the flanges of the W27 \times 123 resist 48% of the beam shear for elastic loading (0.5% drift), which reduces to 40% by 2% drift. Note that from static equilibrium the flange shear force at the column face is equal to the flange shear at the access hole toe. The inclined crack angles of the brittle flange fractures reported by Lee et al. (2005) point to the influence of flange shear in this failure mechanism. Further study is needed to examine more closely the effect of flange shear in RBS connections, particularly for RBS-B connections, which are currently prequalified for use in intermediate moment frames (AISC 2010a).

Strain Distribution in Enhanced WUF-B Connection

The combination of the modified bolt design with the HBS significantly reduces strain demands on the flange in the access hole region during loading at large rotations [illustrated in Fig. 9(b)]. The effect of the HBS can be seen by comparing the strain distribution of the WUF-B with that of the WUF-B w/HBS and by comparing the strain distribution of the all-welded connection with the HBS-W. In both cases the only parameter change is the HBS. The effect of the web connection detail can be seen by comparing the strain distribution of the WUF-B w/HBS with that of the HBS-B and by comparing the WUF-B to the all-welded connection. In both cases

the only parameter change is the web attachment detail. In all of these comparisons it is observed that strain demands are reduced.

When the modified bolt design is combined with the HBS, large deformations from yielding and buckling are shifted away from the connection region. This is illustrated in Fig. 10 where the equivalent plastic strain contours are plotted and compared for the WUF-B [Fig. 10(a)] and the HBS-B [Fig. 10(b)] at a story drift angle of 0.04 radians. Note that in the case of the WUF-B, yielding and buckling is localized to the flanges and access hole, whereas in the HBS-B, the majority of yielding and buckling takes place in HBS where widespread yielding is promoted. This leads to lower strain demands, which are evident by comparing the plastic strain magnitudes. In addition, lower strain demands at the access hole resulted in lower void growth demands when the HBS-B connection was analyzed under the 2010 AISC Seismic Provisions chapter K (AISC 2010b) cyclic loading protocol as shown in Fig. 11. Based upon these results, a large-scale experiment was performed to validate the proposed connection as described in the following.

Experimental Validation

One large-scale exterior type subassemblage (HBS 6) was tested to evaluate the proposed performance-enhancing modifications. For sake of brevity, discussion of the heat-treatment setup,

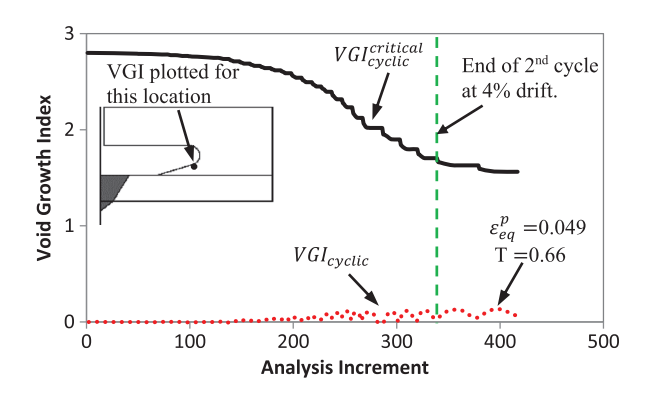


Fig. 11. CVGM prediction for HBS-B; note ε_{eq}^p = equivalent plastic strain; T = stress triaxiality

heat-treatment procedure, field welding, and bolt installation is not provided here. Details of these can be found in Morrison (2015). The test setup and details of the test specimen are shown in Figs. 12(a and b). The W14 × 257 column as shown in Fig. 12(b) satisfies the 2010 AISC *Seismic Provisions* (AISC 2010b) requirements for continuity plates and panel zone shear strength, hence no additional column reinforcement was deemed necessary. In addition, pretest FE simulations predicted limited panel zone yielding (strong panel zone behavior). This ensured that most of the inelastic action was obtained from the beam.

Test Results

Loads were applied at the beam tip in accordance with the 2010 AISC *Seismic Provisions* chapter K (AISC 2010b) cyclic loading protocol. Fig. 13 shows the moment-rotation response of HBS 6, which displays wide hysteresis loops indicating good energy dissipation. The specimen exceeded the 2010 AISC *Seismic*

Provisions (AISC 2010b) SMF qualifying 4% interstory drift angle without significant strength loss. Strength degradation due to local flange, web, and lateral torsional buckling initiated during the 2nd cycle of loading at 4% drift [Figs. 13 and 14(a)] and continued during later loading cycles. Loading of HBS 6 was terminated during the second cycle of loading at 5% drift due to a fracture in the location of significant flange buckling [Figs. 14(a and b)]. This failure mechanism was similar to that observed in all-welded connections and extended end plate connections enhanced with the HBS (Morrison 2015). In all three connections, plastic hinge formation in the HBS was followed by local buckling, strength degradation, and fracture in the location of most severe flange buckling.

The response of HBS 6 is compared to the FE simulation predictions, which show good overall fit of the moment-rotation response [Fig. 13(a)], the amplitude of the strain response measured by a strain gage in the heat-treated region [Fig. 13(b)], and the plastic hinging and local buckling deformations observed in the experiment [Figs. 13(c-f)]. It is noted that while the amplitude of the strain response is reasonably predicted by the simulation, the shift of the mean strain likely caused by the transient yield plateau was not captured [Fig. 13(b)]. Parameters for the CVGM were not available for the heat-treated flange material, so fracture prediction was not attempted. However, the FE model captured the large deformation demands in the region of severe flange buckling, which ultimately led to fracture [Figs. 13(f) and 14(a and b)].

Fig. 15 illustrates the progression of inelastic action along the beam flange via bar graphs in which the distribution of flexural tensile strains (normalized by the yield strain) along the centerline of the beam top flange at various stages of the loading history are plotted. Strains were calculated by postprocessing data obtained from 3D noncontact spatial displacement measurement sensors placed along the beam flange (Morrison 2015). The strain profiles indicate that flexural yielding initiates in the heat-treated areas between 1 and 1.5% story drift [Fig. 15(a)]. As loading is continued, strains increase more in the heat-treated areas than in the regions

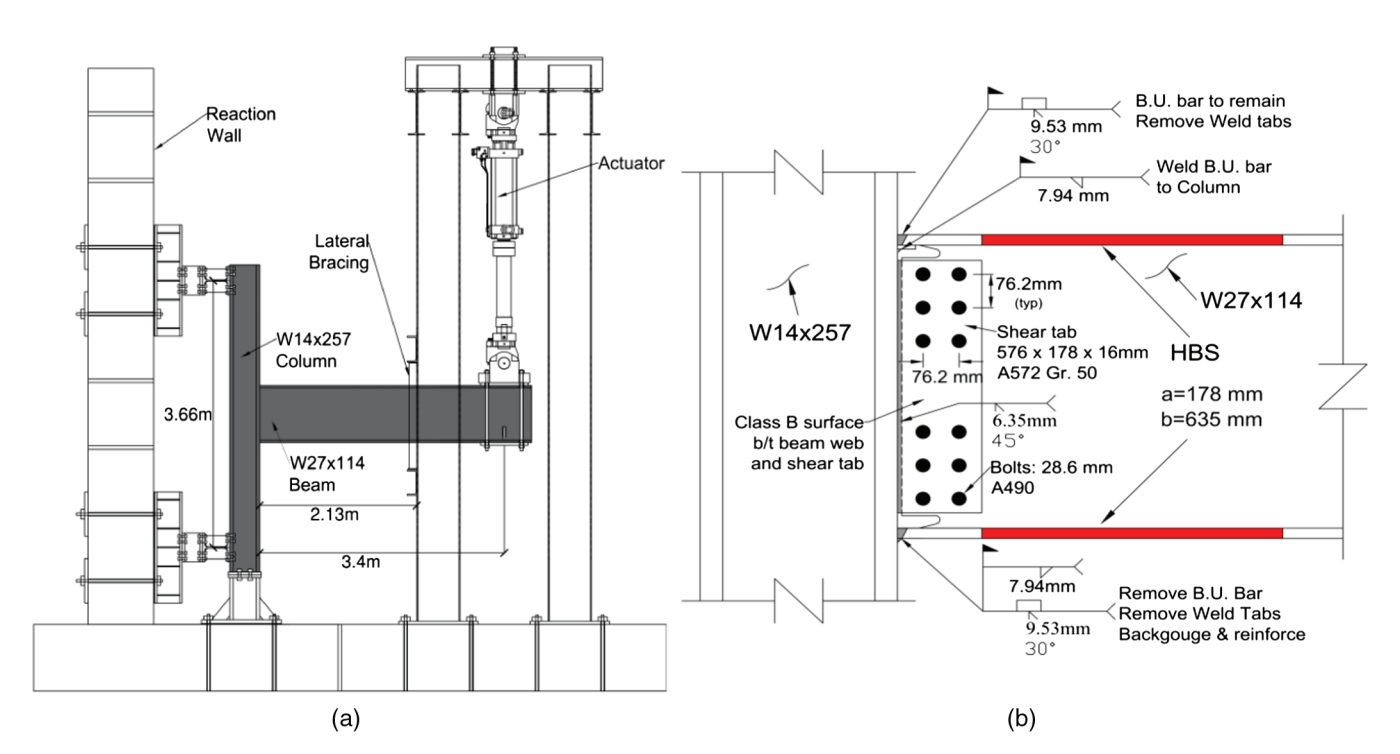


Fig. 12. (a) HBS 6 test setup; (b) HBS 6 connection details

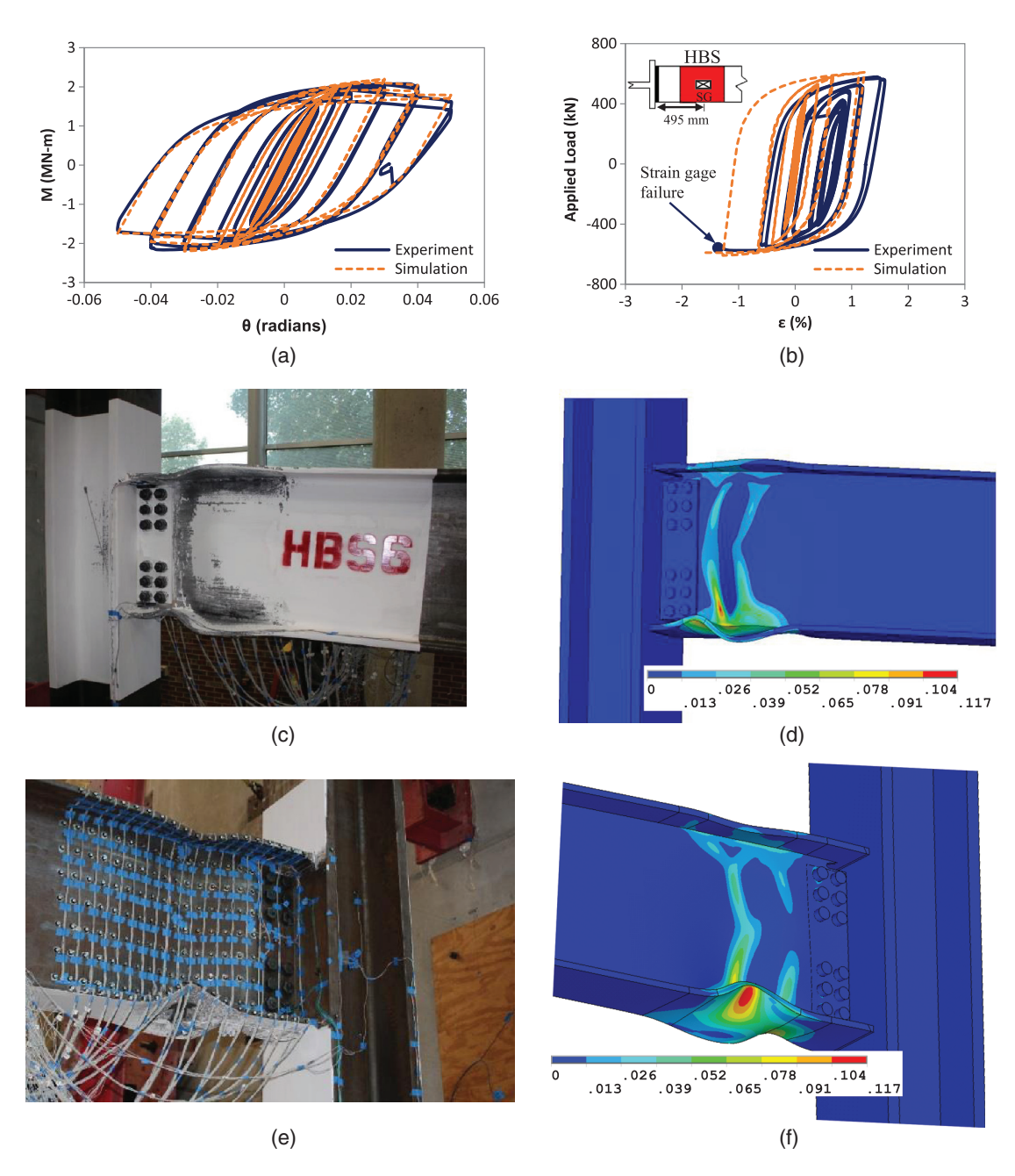


Fig. 13. Comparison of experiment and FE predicted responses for HBS 6: (a) moment-rotation; (b) flexural strain at the center of the bottom flange heat-treated region (location shown in the inset); (c) east view of connection at 5% drift; (d) equivalent plastic strain solution at 5% drift (east view); (e) west view of connection at 5% drift; (f) equivalent plastic strain solution at 5% drift (west view)

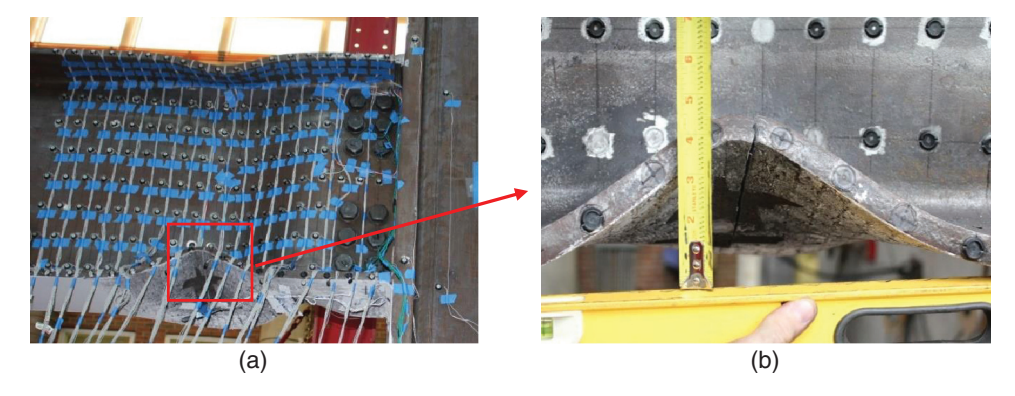


Fig. 14. Local flange buckling and fracture of HBS 6: (a) west view of connection showing beam flange buckling and fracture after test; (b) close-up view of beam flange at location of fracture

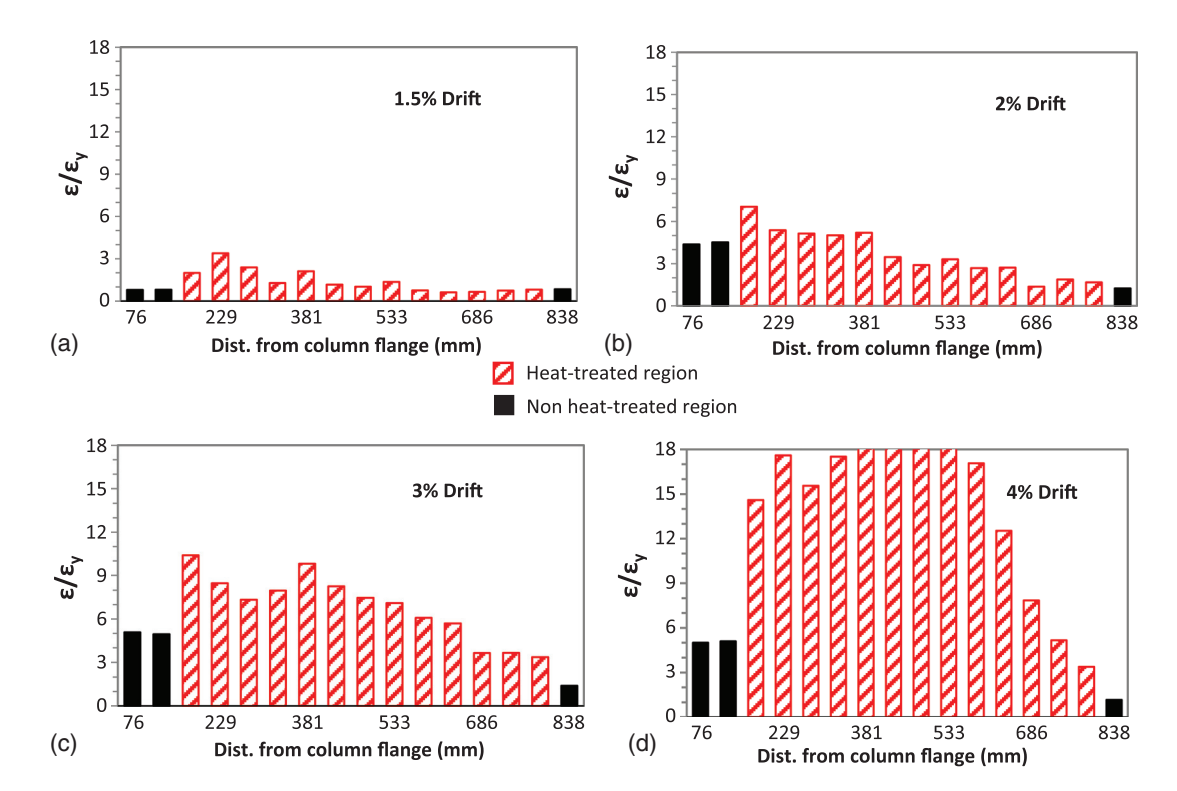


Fig. 15. Recorded flexural strains along HBS 6 beam top flange centerline

adjacent to the beam flange to column flange welds. As drift angles increase from 3 to 4% [Figs. 15(c and d)], strains in the heat-treated regions increase significantly while strains outside of the heat-treated areas grow only slightly. This demonstrates that the large displacements imposed at the beam tip are mostly accommodated by flexural deformation in the HBS. Similar observations have been made in all-welded connections modified with HBS (Morrison et al. 2015). Slight panel zone yielding was observed; however, inelastic panel zone deformations accounted for less than 10% of the total inelastic rotation of the subassemblage.

Future Work on Modified WUF-B Connections

Due to limited resources only one test specimen was evaluated in this study. Future work on the proposed connection needs to be conducted to determine the suitability of this connection over a range of beam and column sizes. Given the high cost of full-scale testing, detailed numerical analysis (such as those outlined earlier) may provide a good starting point for further evaluation.

Conclusion

This study has presented detailed FE analysis and experimental validation of an improved WUF-B moment connection. In addition, detailed FE analysis was used to study the behavior and failure mechanism of post-Northridge WUF-B connections. The analysis showed that the post-Northridge WUF-B connection displays significant bolt slippage beginning at relatively low story drift angles, which leads to a reduction in connection stiffness and bending stress redistribution near the connection. It is observed that bending stresses developed in the beam web are redistributed to the beam flanges adjacent to the access hole, leading to considerably higher flange bending stresses than those experienced by all-welded connections. Web bolt slippage also leads

to increased flange shear stresses adjacent to the access hole, resulting in more local flange bending in the WUF-B. Upon yielding, stress concentrations at the access hole become strain concentrations, which may have led to experimentally observed ductile fracture of the beam flanges.

Detailed finite element analysis showed that, for the connection geometry considered, the modified WUF-B connection, which combines an improved bolt design originally proposed by Lee and Kim (2007), and the recently validated heat-treated beam section (HBS) experienced significantly lower strain demands at the weld access hole when compared to the post-Northridge WUF-B. The modified WUF-B connection was experimentally validated through full-scale testing. The connection displayed ductile response to simulated seismic loading exceeding the 2010 AISC Seismic Provisions (AISC 2010b) SMF qualifying 4% interstory drift angle without significant strength loss. No weld or near-weld cracks were observed. Instead, fracture occurred in the region of significant flange buckling (in the plastic hinge) during cycles at 5% interstory drift. The FE model of the modified WUF-B was validated against the experimental data. Simulation results demonstrate good correlation with the recorded moment-rotation hysteretic response and the observed plastic hinge formation and strength deterioration mechanism.

Acknowledgments

Funding for this research was provided by the National Science Foundation under the Network for Earthquake Engineering Simulation (NSF Grant No. 0936547). However, any opinions presented in this paper are solely those of the authors. In-kind support provided by Steel Fab Inc. and assistance provided by the staff of the Constructed Facilities Laboratory (CFL) at NC State University are gratefully acknowledged.

References

- AISC. (1992). Seismic provisions for structural steel buildings, Chicago.
- AISC. (1997). Seismic provisions for structural steel buildings, Chicago.
- AISC. (2005). Steel construction manual, Chicago.
- AISC. (2010a). Prequalified connections for special and intermediate steel moment frames for seismic applications, Chicago.
- AISC. (2010b). Seismic provisions for structural steel buildings, Chicago. ANSYS 14.5 [Computer software]. ANSYS, Canonsburg, PA.
- ASTM. (2010). "Standard specification for general requirements for rolled structural steel bars, plates, shapes, and sheet piling." ASTM A6-10, West Conshohocken, PA.
- Bruneau, M., Uang, C. M., and Whittaker, A. (1998). *Ductile design of steel structures*, McGraw Hill, New York.
- Chaboche, J. L. (1986). "Time-independent constitutive theories for cyclic plasticity." *Int. J. Plast.*, 2(2), 149–188.
- Engelhardt, M. D., and Husain, A. S. (1993). "Cyclic-loading performance of welded flange-bolted web connections." J. Struct. Eng., 10.1061/ (ASCE)0733-9445(1993)119:12(3537), 3537–3550.
- Engelhardt, M. D., and Sabol, T. A. (1997). "Seismic-resistant steel moment connections: Developments since the 1994 Northridge earthquake." *Prog. Struct. Engng Mater.*, 1(1), 68–77.
- Goel, S. C., Stojadinovic, B., and Lee, H. K. (1997). "Truss analogy for steel moment connections." *Eng. J.*, 34(2), 43–53.
- Han, S. W., Kwon, G. U., and Moon, K. H. (2007). "Cyclic behavior of Post-Northridge WUF-B connections." J. Const. Steel Res., 63(3), 365–374.
- ICBO (International Conference of Building Officials). (1988). Uniform building code, Whittier, CA.
- Iwankiw, N. R., and Carter, C. J. (1996). "The dogbone: A new idea to chew on." Modern Steel Constr., 36(4), 18–23.
- Kanvinde, A. M., and Deierlein, G. G. (2007). "Cyclic void growth model to assess ductile fracture initiation in structural steels due to ultra low cycle fatigue." J. Eng. Mech., 10.1061/(ASCE)0733-9399(2007)133:6 (701), 701–712.
- Kanvinde, A. M., and Deierlein, G. G. (2008). "Validation of cyclic void growth model for fracture initiation in blunt notch and dogbone steel specimens." *J. Struct. Eng.*, 10.1061/(ASCE)0733-9445(2008)134:9 (1528), 1528–1537.
- Kaufmann, E. J., Metrovich, B. R., and Pense, A. W. (2001). "Characterization of cyclic inelastic strain behavior on properties of A572 Gr. 50 and A913 Gr. 50 rolled sections." ATLSS Rep. No. 01-13, National Center for Engineering Research on Advanced Technology for Large Structural Systems, Lehigh Univ., Bethlehem, PA.
- Krawinkler, H., and Popov, E. P. (1982). "Seismic behavior of moment connections and joints." *J. Struct. Div.*, 108(2), 373–391.

- Lee, C.-H., Jeon, S.-W., Kim, J.-H., and Uang, C.-M. (2005). "Effects of panel zone strength and beam web connection method on seismic performance of reduced beam section steel moment connections." *J. Struct.* Eng., 10.1061/(ASCE)0733-9445(2005)131:12(1854), 1854–1865.
- Lee, C.-H., and Kim, J.-H. (2007). "Seismic design of reduced beam section steel moment connections with bolted web attachment." J. Const. Steel Res., 63(4), 522–531.
- Morrison, M. L. (2015). "Innovative seismic performance enhancement techniques for steel building moment resisting connections." Ph.D. dissertation, North Carolina State Univ., Raleigh, NC.
- Morrison, M. L., Schweizer, D. Q., and Hassan, T. (2015). "An innovative seismic performance enhancement technique for steel building moment resisting connections." J. Const. Steel Res., 109(Jun), 34–46.
- Myers, A. (2009). "Testing and probabilistic simulation of ductile fracture initiation in structural steel components and weldments." Ph.D. dissertation, Stanford Univ., Stanford, CA.
- Popov, E. P., Amin, N. R., Louie, J. J. C., and Stephen, R. M. (1985). "Cyclic behavior of large beam-column assemblies." *Earthquake Spectra*, 1(2), 203–238.
- Popov, E. P., and Stephen, R. M. (1972). "Cyclic loading of full-size steel connections." American Iron and Steel Institute, Washington, DC.
- Popov, E. P., Yang, T., and Chang, S. (1998). "Design of steel MRF connections before and after 1994 Northridge earthquake." *Eng. Struct.*, 20(12), 1030–1038.
- Rahman, A., Mahamid, M., Amro, A., and Ghorbanpoor, A. (2007). "The analyses of extended shear tab steel connections—Part I: The unstiffened connections." *Eng. J.*, 44(2), 133–146.
- Richard, R. M., Jay Allen, C., and Partridge, J. E. (1997). "Proprietary slotted beam connection designs." *Modern Steel Constr.*, 37(3), 28–35.
- Sabol, T. A., Engelhardt, M. D., Aboutaha, R. S., Frank, K. H. (1996). "An overview of the AISC Northridge moment connection test program." Proc., 11th World Conf. on Earthquake Engineering, AISC, Chicago.
- SAC. (1998). "Strength and ductility of FR welded-bolted connections." Rep. No. SAC/BD-98/01, Richmond, CA.
- SAC. (2000a). "Behavior and design of radius cut reduced beam section connections." *Rep. No. SAC/BD-00/17*, Richmond, CA.
- SAC. (2000b). "Failure analysis of welded beam to column connections." *Rep. No. SAC/BD-99/23*, Richmond, CA.
- SAC. (2000c). "Parametric tests on the free flange connections." *Rep. No. SAC/BD-00/02*, Richmond, CA.
- SAC. (2000d). "Parametric tests on unreinforced connections. Volume 1—Final report." *Rep. No. SAC/BD-00/01*, Richmond, CA.
- Stojadinović, B., Goel, S. C., Lee, K.-H., Margarian, A. G., and Choi, J.-H. (2000). "Parametric tests on unreinforced steel moment connections." *J. Struct. Eng.*, 10.1061/(ASCE)0733-9445(2000)126:1(40), 40–49.